Available online at www.sciencedirect.com
ScienceDirect
Progress in Biophysics and Molecular Biology 96 (2008) 19–43
Progress in Biophysics & Molecular Biology
www.elsevier.com/locate/pbiomolbio

Review

A guide to modelling cardiac electrical activity in anatomically detailed ventricles

R.H. Clayton[a,*], A.V. Panfilov[b]

[a]Department of Computer Science, University of Sheffield, Regent Court, 211 Portobello Street, Sheffield, S1 4DP, UK
[b]Department of Theoretical Biology, University of Utrecht, The Netherlands

Available online 1 August 2007

Abstract

One of the most recent trends in cardiac electrophysiology is the development of integrative anatomically accurate models of the heart, which include description of cardiac activity from sub-cellular and cellular level to the level of the whole organ. In order to construct this type of model, a researcher needs to collect a wide range of information from books and journal articles on various aspects of biology, physiology, electrophysiology, numerical mathematics and computer programming. The aim of this methodological article is to survey recent developments in integrative modelling of electrical activity in the ventricles of the heart, and to provide a practical guide to the resources and tools that are available for work in this exciting and challenging area.

Keywords: Computer model; Re-entry; Ventricular fibrillation; Ventricle

Contents

*Corresponding author. Tel.: +44 114 222 1845; fax: +44 114 222 1810.
E-mail address: r.h.clayton@sheffield.ac.uk (R.H. Clayton).

0079-6107/$ - see front matter © 2007 Elsevier Ltd. All rights reserved.
doi:10.1016/j.pbiomolbio.2007.07.004

1. Introduction

As a result of the increasing availability of both detailed experimental data and high-performance computers, computational models have begun to be adopted as valuable research tools for various aspects of heart function and dysfunction, including understanding cardiac mechanics, mechanisms of arrhythmias, mechanisms of defibrillation, and improving diagnostic tools by solving the forward and inverse problems of electrocardiography. In each of these research areas, important processes arise at various levels of organisation, from sub-cellular and cellular to the whole organ level, and detailed modelling of these phenomena should be integrative.

An integrative model of whole-ventricle electrophysiology can be assembled from equations that simulate the electrophysiology of a cardiac cell, equations that describe the propagation of the action potential through cardiac tissue, and an anatomically detailed model of ventricular anatomy that includes not only the 3D shape of the ventricles but also the orientation of fibres (Fig. 1). A numerical scheme must then be chosen to solve this hierarchy of models, and a computer program written to integrate them correctly and efficiently. For newcomers to this research area, authoritative review articles are available that cover models at each level of organisation: cellular electrophysiology (Nickerson and Hunter, 2006; Noble and Rudy, 2001; Rudy, 2006), tissue models (Henriquez and Papazogou, 1996; Kleber and Rudy, 2004; Winslow et al., 2001) and models of cardiac anatomy (LeGrice et al., 2001; Vetter and McCulloch, 1998; Winslow et al., 2000).

However, the development of new codes and models requires not only knowledge of what is possible but also the wisdom to choose appropriate components at each level of organisation within the integrative model. For a specific research question it may not be necessary to construct a highly detailed (and expensive to compute) model, and so simplified components can be selected. However, the results will have limitations arising from the simplified components used. The choice of model components is therefore important, so that the detail of the model can be balanced against computational time. However, these choices are not always obvious and the aim of this article is therefore to present a simple practical introduction into this topic, based on the experience of the

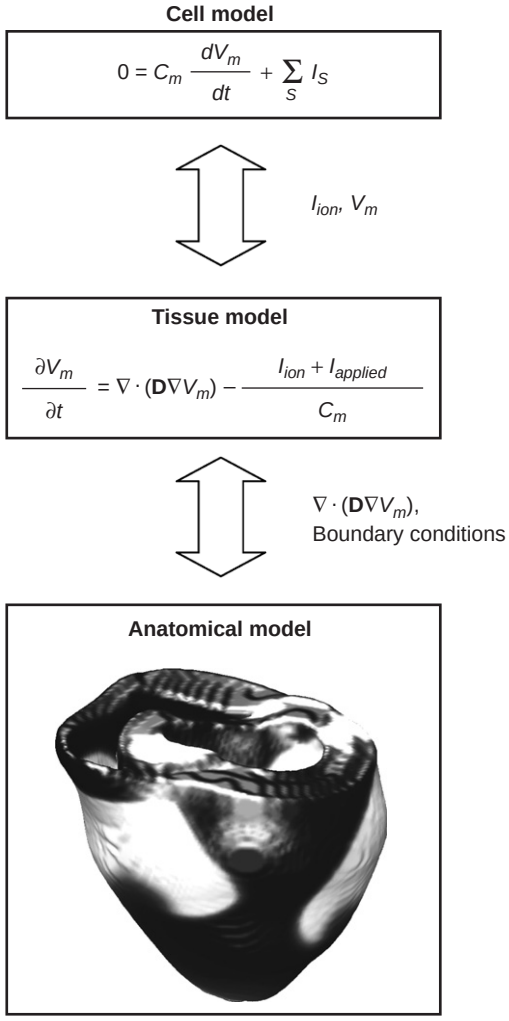

Fig. 1. Integration of different levels in a whole-ventricle model, showing how the models at each level are coupled.

authors. The article is not a comprehensive review covering all aspects of whole heart modelling, but rather it collects together the tools for whole-ventricle modelling that are currently available, with the main emphasis on monodomain models solved with explicit finite difference implementations. The article also explains and discusses the benefits and limitations of different approaches, shows where codes and geometrical models can be obtained, and provides a rationale for making a choice of specific model and method.

We structure our article as follows: For each level of organisation: cell, tissue, and whole ventricle, we (i) provide a brief physiological overview, including the main aspects that are important for the modeller, (ii) discuss the main issues related to modelling at this level, (iii) list the available resources and present our guidelines for choosing an appropriate model, and (iv) give a brief historical overview with suggestions for further reading. Then we discuss numerical and computational issues, and finally we provide some concluding remarks.

2. Cell-level models of membrane excitability

2.1. Physiology

At the cell level, the electrical activity of a cardiac myocyte results from current flow through ion channels and transporters embedded in the cell membrane. Fig. 2(a) shows the equivalent electrical circuit of a patch of

cardiac cell membrane. At rest, ventricular cells maintain a potential difference of about −85 mV across the cell membrane. Figs. 2(b) and (c) show the depolarisation and repolarisation of the cell membrane during an action potential, and illustrate the flow of current carried by Na^+, Ca^{2+} and K^+ ions. The steep upstroke of the action potential results from the rapid opening of Na^+ channels following a stimulus, and the consequent inward flow of Na^+ ions, which depolarises the membrane. This initial event is followed by a smaller inward current carried by Ca^{2+} ions, which, balanced against an outward current carried by K^+ ions, maintains the

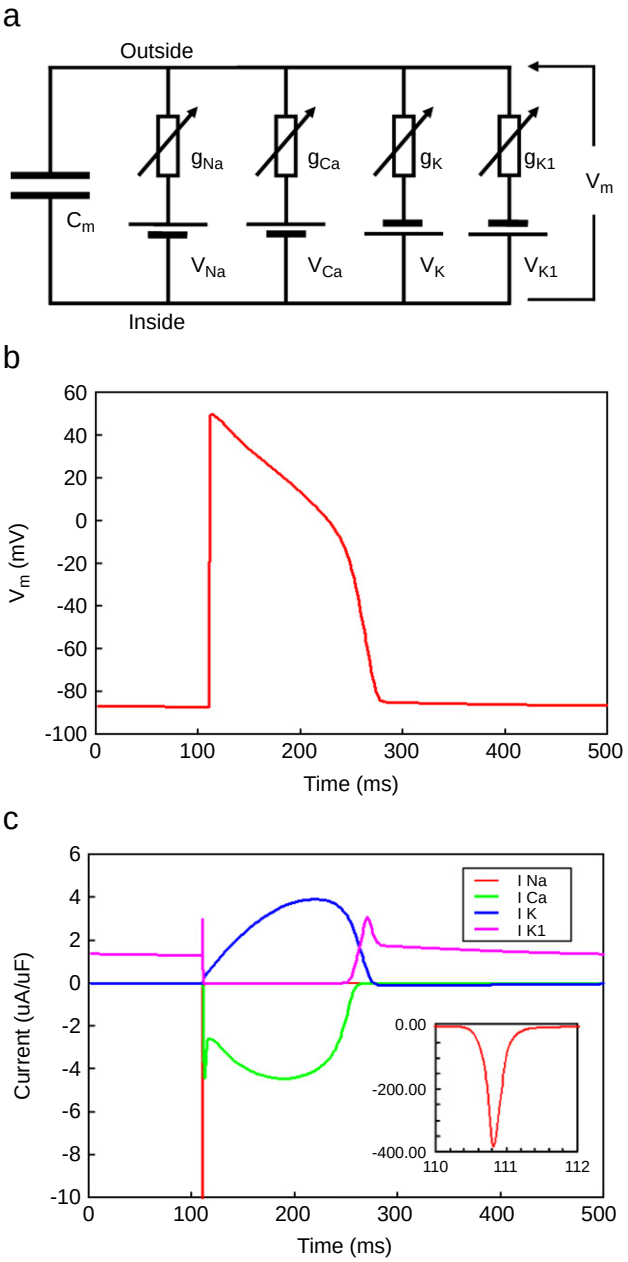

Fig. 2. (a) Simplified equivalent circuit for a patch of cardiac cell membrane. Batteries represent the Nernst potential for each ion (taking into account the permeability of I_K channels to Na^+), variable resistances represent the voltage- and time-dependent ion channel conductance, and the capacitor represents the cell membrane. (b) Example action potential obtained from the LRd cardiac cell model, paced at 500 ms intervals. (c) Corresponding flow of currents carried by Na^+, Ca^{2+} and K^+ ions during the action potential, inset shows the Na^+ current on expanded current and time axes.

plateau phase of the action potential. Finally, the outward current carried by K^+ ions dominates, which results in repolarisation of the cell membrane back to the resting potential.

The action potential duration (APD) is an important characteristic of cardiac cells, and shortens when the cell is stimulated at a higher rate. This property is called APD restitution (Boyett and Jewell, 1980), and, together with conduction velocity (CV) restitution, plays a significant role in the dynamics of propagating action potentials and arrhythmogenesis (Banville and Gray, 2002; Franz, 2003).

2.2. Modelling overview

The total current flow through a membrane patch modelled by the circuit shown in Fig. 2(a) can be expressed as

$$C_{\mathrm{m}} \frac{\mathrm{d}V_{\mathrm{m}}}{\mathrm{d}t} = -\sum_{N} I_n, \tag{1}$$

where ΣI_n is the total transmembrane current, C_{m} the capacitance of the cell membrane per unit area, V_{m} the transmembrane voltage, and I_n are the currents per unit area flowing through N individual ion channels, exchangers and pumps. The currents can be subdivided into two main groups: inward (negative) currents, which depolarise (activate the membrane), and outward (positive) currents, which repolarise the membrane. An additional category of channels are non-selective for cations, and the direction of current flow through these channels depends on membrane voltage. Figs. 2(b) and (c) show the action potential and the major inward and outward currents obtained from the Luo Rudy dynamic model of the guinea pig ventricular myocyte (Luo and Rudy, 1994). The most important inward currents are Na^+ and Ca^{2+} currents, and the most important outward currents are the K^+ current group. There are more than 10 individual currents carried by K^+, each of which has its own conductivity and time dynamics. Most of these ionic currents are controlled by the transmembrane voltage V_{m}; however, another very important regulator is intracellular Ca^{2+} concentration. Intracellular Ca^{2+} directly inhibits the L-type Ca^{2+} channel and contributes directly to the change of V_{m} via the electrogenic NaCa transporter. Modelling of the storage, release and uptake of Ca^{2+} by intracellular stores is an important component of cardiac cell models, but it is complicated because Ca^{2+} release occurs at discrete sites within the cell, and both release and uptake are dependent on the diffusion of Ca^{2+} within the cytosol (Soeller and Cannell, 2004).

Currently there are more than one hundred models of cardiac cells available, which differ both in their complexity and in the level of detail with which they represent the underlying biology (see the model repository at http://www.cellml.org/ for a representative list and description). We give an overview of these models below.

2.3. Currently used and available models

2.3.1. Simplified two-variable models

The simplest types of model are low-dimensional models, which reduce the complex array of ion currents to two variables that describe excitation and recovery. The Fitzhugh Nagumo model (Fitzhugh, 1961) denotes activation and recovery as u and v, where

$$\frac{\partial u}{\partial t} = f(u,v), \quad \frac{\partial v}{\partial t} = g(u,v). \tag{2}$$

These equations can be written in several different styles (Winfree, 1991), but generally $f(u,v)$ is a cubic function of u and a linear function of v, and $g(u,v)$ a linear function of both u and v. This type of model is valuable because the process of excitation and recovery can be analysed in mathematical detail using a phase plane where u is plotted against v (Keener and Sneyd, 1998). Variants of the Fitzhugh Nagumo model have been described that reproduce the rate dependence of action potential duration (Aliev and Panfilov, 1996), and the steady resting potential of cardiac myocytes (Rogers and McCulloch, 1994; Van Cappelle and Durrer, 1980).

2.3.2. First-generation biophysically detailed ventricular cell models

The first generation of cardiac cell models aimed to reproduce the action potential based on available experimental information about the voltage and time dependence of ion channel conductance data, reviewed in Rudy (2006). The ion channel kinetics are based on those used in the Hodgkin–Huxley model of the squid giant axon (Hodgkin and Huxley, 1952), first adapted for cardiac Purkinje cells by Noble (Noble, 1962), and the general form of these models is the following:

$$C_{\mathrm{m}} \frac{\mathrm{d}V_{\mathrm{m}}}{\mathrm{d}t} = -\sum_{S} I_S, \tag{3}$$

$$I_S = \overline{G}_S x_S^1 x_S^2 \ldots x_S^n (V_{\mathrm{m}} - V_S), \tag{4}$$

$$\frac{\mathrm{d}x_S}{\mathrm{d}t} = \frac{x_{S\infty}(V_{\mathrm{m}}) - x_S}{\tau_S(V_{\mathrm{m}})}, \tag{5}$$

where I_S is the current carried by an ionic species S through a particular ion channel, $\overline{G_S}$ the maximal conductance of the ion channel, x_S are the gating variables that vary between 0 and 1 and describe the activation, inactivation and recovery of the ion channel, V_S is the Nernst potential of species S, $x_{S\infty}$ is the steady-state value of a single gating variable x_S (i.e. its value for $\mathrm{d}x/\mathrm{d}t = 0$), and τ_S is a time constant describing the return of x to its steady-state value x_∞ following a voltage perturbation. The voltage dependence of both x_∞ and τ_x can be determined from experimental data (Hodgkin and Huxley, 1952; Rudy, 2006).

The Beeler Reuter model (Beeler and Reuter, 1977) was the first ionic model of ventricular myocytes, as distinct from models of Purkinje cells (McAllister et al., 1975), and it included descriptions of four currents (Na^+, Ca^{2+} and two currents carried by K^+), as well as a greatly simplified model of intracellular Ca^{2+} concentration based on a single ODE. The Luo and Rudy model (Luo and Rudy, 1991) in addition includes a voltage-dependent background current and a voltage-dependent plateau current carried by K^+, as well as a more detailed description of the voltage- and time-dependent K^+ current. This model is often described as the Luo Rudy 1 (LR1) model, and has been extensively used for simulating action potential propagation in tissue because it is relatively easy to modify both APD and APD restitution, and the rate dependence of action potential duration by changing the maximal K^+ conductance, and the maximal conductance and kinetics of the Ca^+ channel gating parameters (Qu et al., 1999). An example of the action potential produced by the LR1 model is shown in Fig. 3(a). Recently, a model which has a complexity similar to LR1 was also proposed for human ventricular cells (TenTusscher and Panfilov, 2006).

2.3.3. Second-generation cardiac cell models

These models, in addition to a biophysically detailed description of ion channel, pump and exchanger currents, also include a detailed description of intracellular Na^+, Ca^{2+} and K^+ concentrations. The general form of these models is as described above, with an additional equation to balance the intracellular and extracellular ion concentrations based on the currents carried by each species:

$$C_{\mathrm{m}} \frac{\mathrm{d}V_{\mathrm{m}}}{\mathrm{d}t} = -\sum_{S} I_S, \tag{6}$$

$$\frac{\mathrm{d}[S]}{\mathrm{d}t} = \sum_{k} I_S^k(V_{\mathrm{m}}, S). \tag{7}$$

The first equation here is similar to that of a first-generation model, but usually includes more ion channel and exchanger currents. The second equation describes the balance of ion S, the concentration of which is affected by k different types of ion channels, pumps and exchanger currents that are carrying this ionic species. An equation of this type is included for each ionic species. Some second-generation models also include an

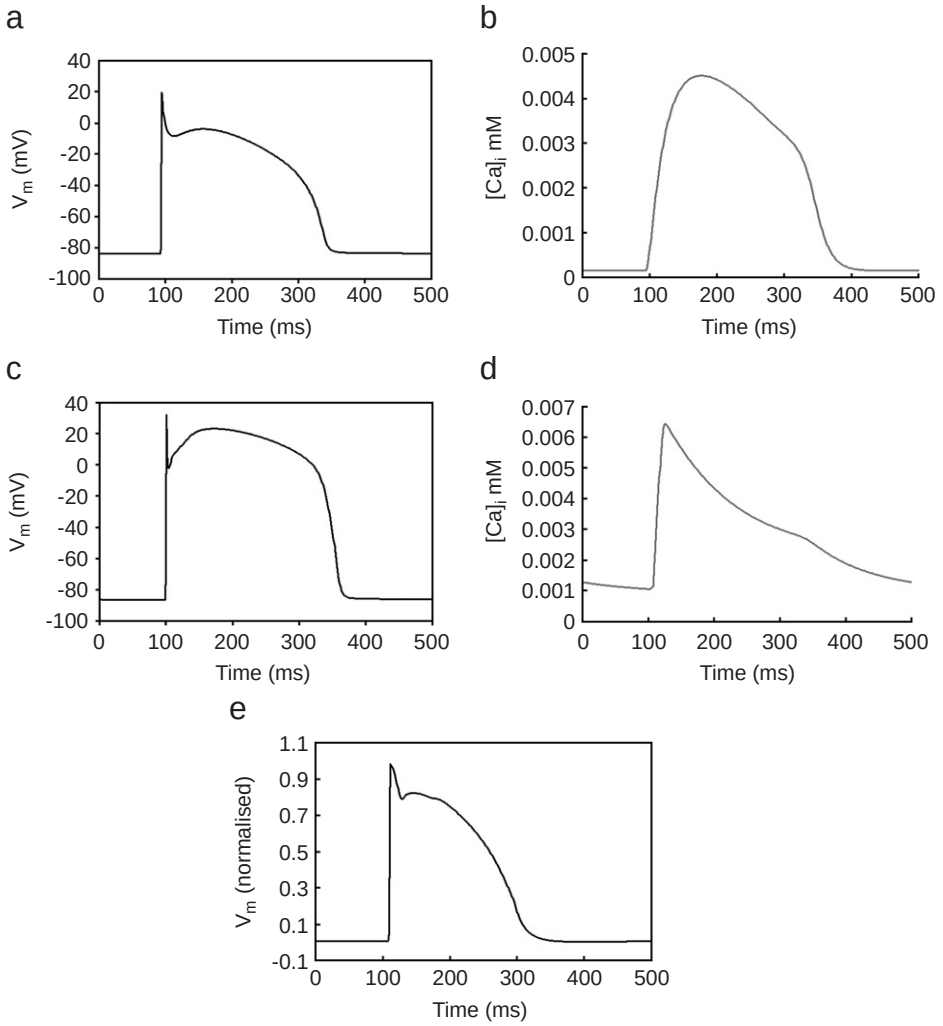

Fig. 3. Action potentials and intracellular Ca^{2+} transient produced by three cell models embedded in a monodomain tissue model of a thin strip (50 × 5 mm) of cardiac tissue, paced at one end at 500 ms intervals. (a) Action potential and (b) Ca^{2+} transient produced by first-generation LR1 model. (c) Action potential and (d) Ca^{2+} transient produced by second-generation TNNP model for human ventricular cells. (e) Action potential produced by reduced 4-variable model, fitted to canine epicardial action potential.

additional description of the subspace and cleft space close to the intracellular and extracellular surfaces of the membrane.

The first second-generation model was the DiFrancesco-Noble model of Purkinje cells (DiFrancesco and Noble, 1985), and other early second-generation models of ventricular cells include the Luo Rudy dynamic (LRd) model (Luo and Rudy, 1994) and the Noble 1998 model (Noble et al., 1998) for guinea pig ventricular cells. The detailed history of the LRd model is documented at http://rudylab.wustl.edu/. There are now many second-generation ventricular cell models (see http://www.cellml.org/), including models for rat (Pandit et al., 2001), rabbit (Puglisi and Bers, 2001), guinea pig (Faber and Rudy, 2000; Luo and Rudy, 1994; Matsuoka et al., 2003; Noble et al., 1998; Viswanathan et al., 1999; Zeng and Rudy, 1995), canine (Fox et al., 2002; Hund and Rudy, 2004; Winslow et al., 1999) and human (Priebe and Beuckelmann, 1998; TenTusscher et al., 2004). Fig. 3(b) shows an example of the action potential produced by the TNNP (TenTusscher et al., 2004) model for human ventricular cells.

Second-generation models are more computationally intensive to solve than first-generation models because they include more state variables for ion channels, pumps and exchangers, as well as the intracellular ion

concentrations and transfer. As a consequence, there has been a simultaneous development of reduced models that capture the key features of the cardiac cell membrane, including excitability, refractoriness and rate-dependent behaviour, without seeking to model the biophysical detail.

2.3.4. Reduced cardiac models

These are distinct from two variable models, because, instead of modelling excitability, activation and recovery in a generic way, these models attempt to greatly simplify the underlying electrophysiology. In the three-variable Fenton Karma model (Fenton and Karma, 1998), the total current flow through the cell membrane is the sum of three currents, a fast inward current corresponding to I_{Na}, a slow inward current corresponding to I_{Ca} and a slow outward current corresponding to I_K. The activation and inactivation of these currents are controlled by three variables u, v and w, with thresholds and time constants that describe general properties, but do not correspond quantitatively and directly with experimental data. Instead, these parameters can be adjusted so that the model can reproduce the action potential shape and the rate dependence of action potential duration obtained for a particular cell type. Example parameter sets are given in publications including Aslanidi et al. (2002), Chen et al. (2005), Cherry and Fenton (2004), Clayton and Holden (2002), Clayton and Taggart (2005), Fenton and Karma (1998) and Fenton et al. (2002).

An extension of this model adds an additional variable (Cherry and Fenton, 2004), to enable a spike and dome action potential morphology to be reproduced, and an example action potential produced by this extended model is shown in Fig. 3(c).

2.4. Which model to choose?

With so many models of cellular electrophysiology available, it is important to understand the benefits and limitations of each kind of model so that an appropriate choice can be made. Biophysically detailed first- and second-generation cell models are generally non-linear and stiff. Numerical solutions are time consuming to obtain when embedded in a tissue model using the approaches described in the next section because it is necessary to use a short time step to resolve rapidly changing variables associated with, for example, the opening of Na^+ channels. This issue is of particular concern for second-generation cell models.

The least time-consuming model to solve is the simplified two-variable type, and the Aliev–Panfilov model (Aliev and Panfilov, 1996) was used for early simulations of ventricular fibrillation in whole-ventricle geometry (Panfilov, 1999; Panfilov and Keener, 1995a). The great advantage of this approach is that simulations can be completed relatively quickly, and that parameters of the model such as action potential duration can be manipulated in a transparent way. Furthermore, phenomena such as meander and instability of a spiral wave observed in tissue simulations using simplified two-variable models are generally also observed in simulations using biophysically detailed models. The main advantage of these models is that they allow us to relate mechanisms to the general overall characteristics of cardiac tissue, for example APD restitution and CV restitution. However, the inherent simplification of these models means that they cannot provide any insight into the behaviour and influence of specific ion channels and other intracellular processes on propagation because they are not included. Thus two-variable models should be used to study wave propagation in the heart where the aim is to determine general effects or to get the result in the shortest possible time. This approach is potentially valuable, for example, for patient-specific modelling (Sermesant et al., 2006), which requires multiple adjustments of the models to each specific situation and does not require reproduction of all biophysical details.

Reduced models offer a closer link to real tissue than two-variable models. Time and voltage can be scaled appropriately, without the computational complexity of the first-generation biophysically detailed models. Both the action potential shape and its rate dependence can be fitted to experimental data, so that the characteristics of a particular tissue can be simulated. This approach has been used for simulations of ventricular fibrillation in whole-ventricle geometry (Clayton and Holden, 2004). The guidelines for application of these models are similar to those for two-variable models, with slightly lower numerical efficiency on one hand, but with a more detailed match of the overall properties of cardiac cells on the other.

First-generation models have been widely used for studies of ventricular re-entry and fibrillation in simplified (Garfinkel et al., 2000; Qu et al., 1999, 2000) geometries, and the modified LR1 model has also been used for whole-ventricle simulations (Xie et al., 2004). First-generation models give a good balance between numerical efficiency and biophysically important detail, and we consider them to be the best approach available at present.

Second-generation models include sufficient detail to enable a detailed mechanistic study of phenomena including the action of drugs on specific ion channels and the consequences of channelopathies (Clancy and Rudy, 1999, 2001), the mechanisms of after-depolarisations (Faber and Rudy, 2000; Viswanathan and Rudy, 1999; Zeng and Rudy, 1995) and the development of regional ischaemia (Ferrero et al., 2003; Shaw and Rudy, 1997). However, whole-ventricle simulations using second-generation cell models are at the 'top end' of anatomically detailed modelling. So far studies involving these models have largely been confined to the smaller mouse and rabbit hearts, where they have been used to examine the effects of electrotonic current flow in the rabbit and mouse heart (Sampson and Henriquez, 2005) and defibrillation in the rabbit heart (Trayanova, 2006).

Translating cell models from a description in a journal article to correct code is not always easy due to errors associated with publication, particularly in the type setting of equations. Code for some models is available online, and structured languages based on XML for describing model equations and parameters have been developed recently (Lloyd et al., 2004; Nickerson and Hunter, 2006). Languages such as CellML (see www.cellml.org) have the capacity for built-in checking of units and consistency, and for automated code generation. The growing database of models available in CellML is likely to resolve many of the problems associated with coding cardiac cell models.

Finally, let us list several problems that have been found in studies involving second-generation ionic models. A specific problem arises due to linear or non-linear interactions between the equations of second-generation models, which may result in dependence of solutions on initial conditions, for example, the initial distribution of Ca^{2+} within the cell. This problem may be manifested by the accumulation of ions in the intracellular or extracellular space, leading to instability (Hund et al., 2001). Another recent finding is that two cell models, developed independently from experimental data but describing cells of the same type, may show very different behaviour in tissue (Cherry and Fenton, 2007). This is a rather complex issue, and highlights the need for not only careful validation of second-generation models but also an understanding of the parameter sensitivity of the model equations, and how this influences tissue-level behaviour. A related problem with second-generation models is that many of the parameters used to describe the function of ion channels, pumps and exchangers as well as intracellular handling of Ca^{2+} are extremely difficult to measure. Some expressions and parameters may therefore use data from other species, and the provenance of components in a particular model may not always be clear. These parameters may also have been obtained at temperatures other than 37 °C, and under stable voltage clamp conditions rather than the dynamic and repetitive changes in V_m involved in the action potential. Therefore, although second-generation ionic models will be a good approach in anatomical modelling in the future, implementation of these models at the present time requires substantial time not only for whole-ventricle computations, but also for understanding of the chosen model and its limitations in simple geometries.

2.5. Historical notes and further reading

The present generation of cardiac cell models is based on the Hodgkin–Huxley model of the squid giant axon (Hodgkin and Huxley, 1952), first adapted for cardiac Purkinje cells by Noble (Noble, 1962). The background and history of the development of these models has been reviewed (Nickerson and Hunter, 2006; Noble and Rudy, 2001; Puglisi et al., 2004; Rudy, 2006), together with what is known about the structure and function of cardiac ion channels, pumps and exchangers (Boyett et al., 1996; Carmeliet, 1999; Roden et al., 2002), and the details of intracellular Ca^{2+} handling (Bers, 2002; Bers and Guo, 2005; Eisner et al., 2000). A more recent development has been the use of Markov state-based models for describing ion channel behaviour (Clancy and Rudy, 1999, 2001).

3. Tissue-level models of action potential propagation

3.1. Physiology

An action potential propagates along the cell membrane because of depolarising local current flow ahead of the action potential upstroke. This depolarisation opens Na^+ channels, and hence initiates the subsequent action potential. Cardiac myocytes are coupled to each other by gap junctions, and organised in fibres, which in turn are organised in sheets. The fibre and sheet orientation varies throughout the ventricles (LeGrice et al., 1995; Nielsen et al., 1991; Streeter, 1979). Propagation of the action potential is two to three times faster in the fibre direction than orthogonal to it, and propagation orthogonal to sheets is believed to be two to three times slower than orthogonal to fibres (Hooks et al., 2002).

3.2. Modelling overview

The granular nature of cardiac tissue may have an important effect on action potential propagation at the cell scale (Kleber and Rudy, 2004), but most models assume that tissue can be represented either as a regular arrangement of excitable units connected by intracellular and extracellular resistances (Conrath et al., 2004; Gima and Rudy, 2002) or as a functional syncytium where membrane voltage is assumed to propagate smoothly. We concentrate on the latter type of model below.

3.3. Currently used and available models

3.3.1. Monodomain model

This approach assumes that cardiac tissue behaves as an excitable medium, with diffusion and local excitation of membrane voltage. It provides the simplest description of action potential propagation:

$$\frac{\partial V_{\mathrm{m}}}{\partial t} = \nabla \cdot (\mathbf{D} \nabla V_{\mathrm{m}}) - \frac{I_{\mathrm{ion}} + I_{\mathrm{applied}}}{C_{\mathrm{m}}}. \tag{8}$$

Here ∇ is the gradient operator, and $\mathbf{D}$ is a coefficient with units of distance^2 time^{-1} that describes the effective diffusion of voltage through the medium. The currents I_{ion} and I_{applied} are conventional, so they represent the flow of positive ions from inside to outside the cell (i.e. flow of Na^+ into the cell during the action potential upstroke is a negative current) through the membrane and any applied stimulus, respectively. For models of isotropic tissue $\mathbf{D}$ is a scalar quantity D, and is given by

$$D = \frac{1}{S_v R_i C_{\mathrm{m}}} = \frac{G_i}{S_v C_{\mathrm{m}}}, \tag{9}$$

where S_v is the surface volume ratio of cells, R_i the bulk cytoplasmic resistivity of the tissue, C_{m} the specific capacitance and G_i the bulk intracellular conductivity.

Cardiac tissue anisotropy in monodomain models is given by the diffusion tensor $\mathbf{D}$ (related to conductivity by Eq. (9)), which can be found from the fibre direction and orientation of the sheet plane and is discussed in more detail in Section 4.5.

3.3.2. Bidomain model

In contrast to the monodomain described above, the bidomain approach considers cardiac tissue as a two-phase medium comprising intracellular and extracellular spaces. The transmembrane potential in bidomain model is the difference between the intracellular and extracellular potentials:

$$V_{\mathrm{m}} = \Phi_{\mathrm{i}} - \Phi_{\mathrm{e}}. \tag{10}$$

The overall system of bidomain equations is the following (Gulrajani, 1998; Henriquez and Papazogou, 1996; Roth, 2004):

$$\nabla \cdot (\mathbf{G}_{\mathrm{i}} + \mathbf{G}_{\mathrm{e}}) \Phi_{\mathrm{e}} = -\nabla \cdot (\mathbf{G}_{\mathrm{i}} \nabla V_{\mathrm{m}}), \tag{11}$$

$$\nabla \cdot (\mathbf{G}_i \nabla V_m) + \nabla \cdot (\mathbf{G}_i \nabla \Phi_e) = -S_v I_m, \tag{12}$$

$$I_m = C_m \frac{dV_m}{dt} + I_{ion}, \tag{13}$$

where the subscripts i and e denote the intracellular and extracellular spaces, respectively, I_m is the current flow through the membrane per unit area, $\mathbf{G}$ the conductivity tensors, S_v the surface to volume ratio for cells, I_m the membrane current per unit area, and $I_{applied}$ the currents injected into the intracellular and extracellular spaces.

This system consists of coupled parabolic and elliptic differential equations. The bidomain equations are much more difficult than the monodomain equation to integrate numerically because the full elliptic problem must be solved for each time step of the parabolic equation. One of the most promising finite difference approaches for this problem was proposed by Keener and Bogar (1998). This is based on a combination of a multigrid approach and the Crank Nicolson method. Other approaches based on finite elements have also been proposed (Austin et al., 2006; dos Santos et al., 2004; Vigmond et al., 2002), and a fuller discussion is provided elsewhere in this issue (Vigmond et al., 2007).

3.4. Which model to choose?

The bidomain approach considers the extracellular and intracellular spaces explicitly, and hence provides a more detailed model of cardiac tissue than the monodomain model. However, an obvious advantage of monodomain models is their numerical efficiency: in some cases monodomain models can be ten or more times faster for simulation of the same problem compared to bidomain models. For simulation of wave propagation in the heart, monodomain models reproduce many of the phenomena that are observed experimentally, and are thus an appropriate tool. Monodomain models are the main focus of the present article.

However, the more detailed description of tissue offered by the bidomain equations is necessary to model phenomena where these have an important influence. For example, during defibrillation, current is injected into the extracellular space, and the unequal anisotropy of extracellular and intercellular domains produces patterns of polarisation and depolarisation that are observed experimentally, and which can be accounted for in bidomain models only (Trayanova, 2006). There are also some data that suggest that the behaviour of re-entrant waves close to the tissue surface may be different in monodomain and bidomain models (Sambelashvilli and Efimov, 2004).

The numerical implementation of monodomain models together with anatomically detailed models of fibre orientation within the ventricles is described in Section 5.

3.5. Historical notes and further reading

Cardiac cells are discrete entities, linked by gap junctions at specific locations. The simplest representation of action potential propagation is a cellular automaton, where nodes (cells) on a spatially extended grid possess a state which is updated at successive time steps. A simple cellular automaton was used as a very early model of excitation in atrial cardiac tissue (Moe et al., 1964); more recently, this approach has been used to model electrical activation in whole-ventricle geometries (Wei et al., 1995), and in geometries representing heterogeneous tissue (Bub et al., 2002). The development and biophysical principles underlying models of discrete and continuous cardiac tissue have been described in a thorough review by Kleber and Rudy (2004), and the effects of discrete cardiac tissue structure have been examined by Stinstra et al. (2005).

4. Whole-ventricle anatomical models

4.1. Anatomy

The cardiac ventricles are thick walled compared to the atria, and possess a fibrous structure with spatially varying fibre orientation (Streeter, 1979). Cardiac fibres are arranged into sheets, which are separated by

cleavage planes (LeGrice et al., 1995). Within the ventricular wall, cardiac tissue is composed of myocytes interwoven with other cells and structures, predominantly fibroblasts (Camelleti et al., 2005).

4.2. Modelling overview

Whole-ventricle models of electrical activity require the three-dimensional geometry of the ventricles, together with a description of the orientation of fibres. It is possible to use simplified models to investigate generic features of propagation, where the ventricular geometry is abstracted to a slab representing a piece of the ventricular wall (Clayton and Holden, 2003; Panfilov and Keener, 1993; Taccardi et al., 2005) or a spherical geometry (Chavez et al., 2001; Rohlf et al., 2006).

Early models of human ventricle geometry were based on dissection of anatomical specimens, but did not include a description of fibre orientation (Miller and Geselowitz, 1978; Okajima et al., 1968). High-resolution dissection and histology has been used to determine both geometry and fibre orientation in the rabbit (Vetter and McCulloch, 1998), canine (Nielsen et al., 1991) and pig (Stevens et al., 2003) ventricle. In these models, the measurements are fitted to a finite-element description where the finite elements describe the 3D geometry, and the fibre orientation is expressed as a set of direction cosines that varies smoothly as a field within each element. Initially these descriptions used a system of prolate spheroidal co-ordinates. This approach provides an ideal co-ordinate system for fitting because the prolate spheroid is a good first approximation of the shape of the ventricles, and a linear least-squares algorithm can be used, in which only the radial co-ordinate is fitted. The finite element description in prolate spheroidal co-ordinates can be converted to a regular Cartesian grid, where each point in the grid is defined as either inside or outside the tissue, and points that are inside possess a fibre orientation that is interpolated from the finite element description.

With the development of high-strength magnets offering high-resolution magnetic resonance imaging (MRI) and techniques such as diffusion tensor MRI (DTMRI) (Le Bihan et al., 2001), it has become possible to obtain anatomically detailed models without dissection. Since MRI images are typically obtained in tissue slices and assembled into a 3D volume representation, this approach lends itself to a description based on a Cartesian grid.

4.3. Currently used and available models

4.3.1. UCSD rabbit anatomy (Vetter and McCulloch, 1998)

This geometry was obtained by fixing a rabbit heart mechanically, filling the ventricles with silicone, slicing the ventricles and imaging each slice. Each image was then segmented into regions inside and outside the tissue. Tissue blocks were extracted from these slices, and fibre orientation was determined. Data were fitted to a bicubic Hermite finite element description in prolate spheroidal co-ordinates. This geometry is available as part of the *Continuity* package, which can be downloaded for academic use from http://cmrg.ucsd.edu/Continuity. Figs. 4(c) and (d) show views of the anatomy and fibre orientation in this model.

4.3.2. Auckland canine ventricle (Nielsen et al., 1991)

Canine hearts were fixed mechanically, and the ventricles filled with silicone. In two hearts, 0.5 mm thick layers of epicardium were progressively removed, and fibre orientations were measured on the exposed surface with a spatial resolution of between 2.5 and 5 mm. These data, together with measurements of the epicardial and endocardial surfaces, were fitted to bicubic Hermite finite element descriptions in prolate spheroidal co-ordinates. Initially the data were fitted to a 24-element mesh, but additional elements were also introduced to resolve sharp gradients in fibre orientation at the apex and the border between right ventricle and the septum. A later study also established the alignment of sheets within the ventricular wall (LeGrice et al., 1995), and more recent work has also fitted the original data to a 48-element model with tricubic elements in regular Cartesian co-ordinates (Usyk et al., 2002). This canine geometry is available for academic use, together with the CMISS package, from http://www.cmiss.org/. Figs. 4(a) and (b) show views of the anatomy and fibre orientation in the later 48-element model.

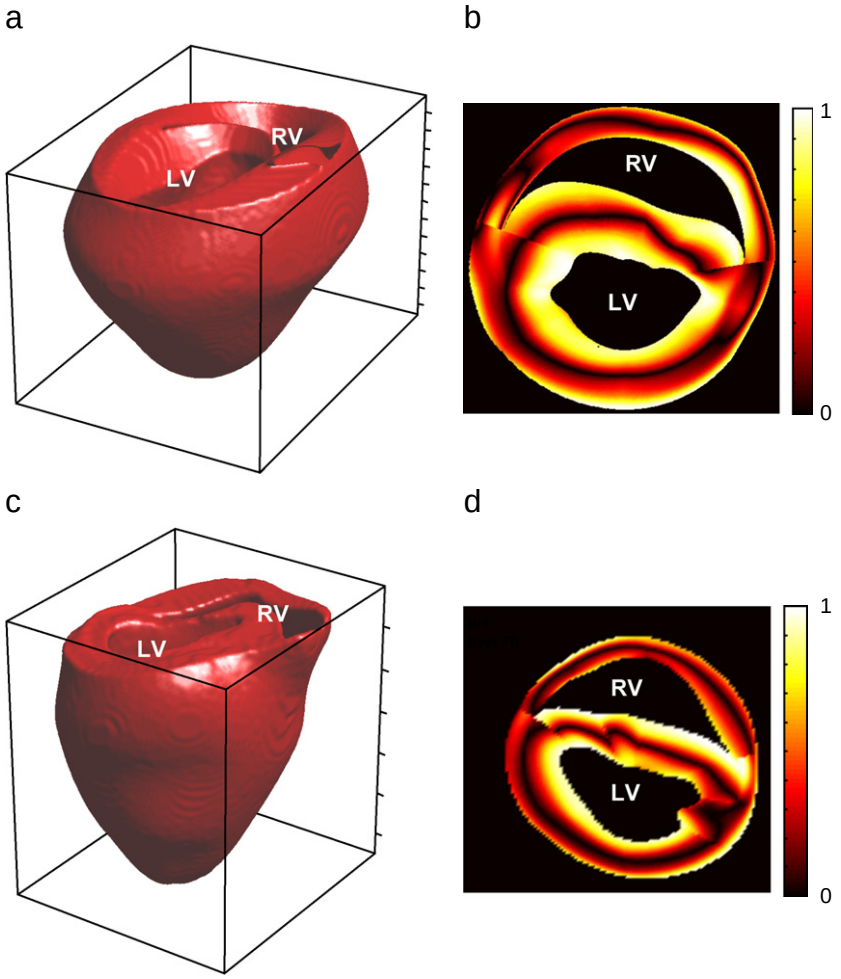

Fig. 4. Visualisation of (a,b) Auckland canine and (c,d) UCSD rabbit ventricles showing (a,c) anatomy, and (b,d) fibre orientation in a short-axis section where the colour coding shows the direction cosine of fibre orientation relative to the long axis on the left ventricle. Discontinuities in fibre orientation at the junction of the right ventricle and the septum can be seen.

4.3.3. *Auckland pig ventricle (Stevens et al., 2003)*

This model was constructed in a similar way to the canine model, although the starting point for the fitting process was a representation of the valve rings at the base of the ventricles, and the finite element description uses tricubic Hermite elements in rectangular Cartesian co-ordinates.

4.3.4. *Models based on MRI data*

Human MRI data have been used to construct a model of human ventricles that included fibre orientation fitted from the Auckland canine model (Hren et al., 1998).

A more recent development has been anatomical models that are being developed based on non-invasive MRI data. The technique of DTMRI measures the Brownian motion of water molecules, which, in an anisotropic medium such as cardiac tissue, is constrained to some extent by the tissue structure (Le Bihan et al., 2001). This approach was first used to image tissue blocks from the canine ventricles, which were then correlated with histological analysis (Hsu et al., 1998). Further studies assessed the variability of fibre orientation in equatorial slices taken from the goat ventricles (Geerts et al., 2002), and rabbit and canine ventricles (Scollan et al., 2000). Construction of 3D models with fibre orientation has followed, for the mouse (Henriquez et al., 2004) and canine (Helm et al., 2005; Zhukov and Barr, 2003) ventricles. Canine ventricle

models for normal and failing hearts are available for academic use from the Johns Hopkins group at http://www.ccbm.jhu.edu/research/dSets.php. It should be noted, however, that MRI data provide only grey scale images, and show regions that contain not only excitable cells but also connective tissue and sometimes also devices that are used to support the ventricle within the imaging chamber. Automated segmentation of the true heart geometry from these data is not a trivial procedure because the greyscale does not distinguish between myocardial and connective tissue and it may in addition be non-uniform between slices. One solution to this problem is to combine high-resolution MRI with histology data from the same specimen, enabling precise and guided segmentation. Recent studies show that this approach is capable of producing very finely detailed models of the rabbit ventricle (Burton et al., 2006).

4.4. Implementing diffusion and conductivity tensors

Most whole-ventricle simulations assume axially symmetric anisotropy, in which the diffusion in all directions orthogonal to the fibre direction is assumed to be the same. In this case there are just two principal values of the effective diffusion coefficient (or conductance), the longitudinal coefficient $D_{||}$, which describes propagation along the fibres, and the transverse coefficient $D_{\perp}$, which describes propagation orthogonal to the fibres. If $\mathbf{A}$ is a unit vector giving the fibre direction (i.e a vector of direction cosines), then the diffusion tensor can be written as

$$\mathbf{D} = D_{\perp}\mathbf{I} + (D_{||} - D_{\perp})\mathbf{A}\mathbf{A}^{\mathrm{T}}, \tag{14}$$

where $\boldsymbol{I}$ is the identity matrix, and $\mathbf{A}^{\mathrm{T}}$ is the transpose of $\mathbf{A}$. Thus the elements of the effective diffusion tensor $\mathbf{D}$ can be written (Panfilov and Keener, 1995b, Fenton and Karma, 1998) as

$$d_{ij} = \begin{cases} D_{\perp} + (D_{\parallel} - D_{\perp})a_i a_j & (i = j), \\ (D_{\parallel} - D_{\perp})a_i a_j & (i \neq j). \end{cases} \tag{15}$$

For the case of orthotropic anisotropy with three principal directions (Hooks et al., 2002), the equivalent expression for the diffusion tensor will be

$$\mathbf{D} = D_{||}\mathbf{A}\mathbf{A}^{\mathrm{T}} + D_{\diamond}\mathbf{B}\mathbf{B}^{\mathrm{T}} + D_{\perp}\mathbf{G}\mathbf{G}^{\mathrm{T}}, \tag{16}$$

where $D_{||}$, $D_{\diamond}$ and $D_{\perp}$ are diffusion coefficients along the fibres, orthogonal to fibres in the sheet plane, and orthogonal to fibres and sheets, and $\mathbf{A}$, $\mathbf{B}$ and $\mathbf{G}$ are unit vectors in the corresponding directions.

4.5. Which model to choose?

The choice of anatomical model solely depends on the research question and experimental data set against which the computations will be verified. Currently, the most commonly used is the Auckland canine ventricle model; however, at present, increasing numbers of studies involve the UCSD rabbit geometry, Auckland pig geometry and human anatomical models, which have obvious clinical advantages.

4.6. Historical notes and further reading

The whole-ventricle models described in this section have been used for a variety of studies that have focussed on normal beats, arrhythmias and electromechanical coupling. These include use of the Auckland canine anatomy to simulate normal beats and re-entrant ventricular fibrillation using several different models of excitation (Berenfeld and Pertsov, 1999; Clayton and Holden, 2004; Clayton et al., 2006; Gray and Jalife, 1998; Panfilov, 1999; Panfilov and Keener, 1995a; Xie et al., 2004). The UCSD rabbit anatomy has also been used to investigate arrhythmias (Cherry and Fenton, 2004; Rogers, 2002), defibrillation (Rodriguez et al., 2006; Trayanova, 2006) and electrotonic current flow (Sampson and Henriquez, 2005).

5. Numerical methods and computational issues

5.1. Overview

Whole-ventricle simulations involve solving stiff ODE systems representing excitability, embedded within the monodomain or bidomain equations that in turn are solved across detailed descriptions of cardiac ventricular anatomy. These are complex computational tasks, and there are important choices to be made, as well as opportunities to optimise the computations. In this section we concentrate first on methods for solving the cell model ODE system. Following this, we discuss approaches to solving the monodomain and bidomain tissue models. Finally we consider the decomposition of whole-ventricle simulations for use with high-performance parallel computers.

Throughout this section we focus on the explicit finite difference methods that have been widely used for simulating cardiac electrical activity (Panfilov, 1997; Xie et al., 2004). Other approaches have been used to solve the monodomain and bidomain tissue models, and these include methods based on finite elements (Austin et al., 2006; Colli Franzone et al., 2006; Rogers, 2002; Rogers and McCulloch, 1994; Vigmond et al., 2002), finite volumes (Harrild et al., 2000; Trew et al., 2005) and combinations of these (Buist et al., 2003). Finite element and finite volume approaches offer some advantages over finite differences, especially for modelling boundary conditions at the curved surfaces of the heart (Austin et al., 2006). However, finite element methods are generally more difficult to implement, and more computationally intensive to solve.

5.2. Cell model ODEs

Biophysically detailed cardiac cell models are generally described by Eq. (3), and the gating variables for both first- and second-generation cardiac cell models are described by the voltage-dependent terms $x_\infty(V_\mathrm{m})$ and $\tau_x(V_\mathrm{m})$, as described in Eq. (5) above. Several finite difference solution schemes including explicit Euler, fourth-order Runge-Kutta and implicit techniques (Press et al., 1992) have been used to solve these equations, but the most widely used approach has been the discrete form proposed by Rush and Larsen (1978):

$$x_{n+1} = x_\infty(V_n) + (x_n - x_\infty(V_n))\mathrm{e}^{-\Delta t/\tau_x(V_n)}. \tag{17}$$

Here V_n is the membrane voltage at time step n, and Δt is the time step. This approach has the important advantages of improved accuracy. Furthermore, the voltage-dependent terms $x_\infty(V_\mathrm{m})$ and $\tau_x(V_\mathrm{m})$ can be pre-computed and stored in a lookup table, improving computational efficiency.

At each time step, the membrane currents, described by equations of the form of (4), can be computed, and the new value of membrane voltage can be calculated from Eq. (3).

5.3. Finite difference solutions of the monodomain tissue model

For models of isotropic tissue, the effective diffusion coefficient D is a scalar. The diffusion term of the monodomain equation (Eq. (8)) can therefore be written for a Cartesian co-ordinate system as

$$\nabla \cdot \mathbf{D}\nabla V_\mathrm{m} = D\nabla^2 V_\mathrm{m} = D\left[\frac{\partial^2 V_\mathrm{m}}{\partial x^2} + \frac{\partial^2 V_\mathrm{m}}{\partial y^2} + \frac{\partial^2 V_\mathrm{m}}{\partial z^2}\right]. \tag{18}$$

For a regular Cartesian grid, the second-order derivative can be written in finite difference form as

$$\frac{\partial^2 V_\mathrm{m}}{\partial x^2} = \frac{V(x+\Delta x, y, z) - 2V(x, y, z) + V(x-\Delta x, y, z)}{\Delta x^2}. \tag{19}$$

For anisotropic tissue with axial symmetry $\mathbf{D}$ is a diffusion tensor, so for a Cartesian coordinate system x_1, x_2, x_3 the diffusion term becomes

$$\nabla \cdot \mathbf{D}\nabla V_\mathrm{m} = \sum_{i=1}^{3}\sum_{j=1}^{3}\frac{\partial}{\partial x_i}\left(d_{ij}\frac{\partial V_\mathrm{m}}{\partial x_j}\right) = \sum_{i=1}^{3}\sum_{j=1}^{3}\left(\frac{\partial d_{ij}}{\partial x_i}\frac{\partial V_\mathrm{m}}{\partial x_j} + d_{ij}\frac{\partial^2 V_\mathrm{m}}{\partial x_i \partial x_j}\right). \tag{20}$$

The elements d_{ij} are given in terms of the effective diffusion coeffients for longitudonal and transverse propagation $D_{||}$ and $D_{\perp}$, and the local fibre orientation cosines a_1, a_2 and a_3. The derivatives of these elements are given by (Panfilov and Keener, 1995a, b; Fenton and Karma, 1998)

$$\frac{\partial d_{ij}}{\partial x_i} = (D_{||} - D_{\perp})\left(a_i \frac{\partial a_j}{\partial x_i} + a_j \frac{\partial a_i}{\partial x_i}\right). \tag{21}$$

In a numerical scheme, these derivatives can be precomputed and stored at the beginning of a simulation.

To approximate all the derivatives in Eq. (20), we need to compute, in addition to the second derivatives approximated by (19), the first derivatives and the cross-derivatives. For a space step Δx, a numerical approximation can then be achieved as

$$\frac{\partial V}{\partial x} \approx \frac{V(x+\Delta x, y, z) - V(x-\Delta x, y, z)}{2\Delta x}, \tag{22}$$

$$\frac{\partial^2 V}{\partial x \partial y} = \frac{[V(x+\Delta x, y+\Delta y, z) - V(x+\Delta x, y-\Delta y, z)] - [V(x-\Delta x, y+\Delta y, z) - V(x-\Delta x, y-\Delta y, z)]}{2\Delta x 2\Delta y}, \tag{23}$$

with similar expressions for the derivatives in other directions.

5.4. Selection of diffusion coefficient, time step and space step

The choice of time step, space step and diffusion coefficient has important implications for not only the stability of a particular scheme but also the computational time it will take to solve.

For the cell model, a time step must be chosen that will resolve not only the sharp upstroke of the action potential but also the release of Ca^{2+} from intracellular stores in second-generation models. A typical time step for the Rush and Larsen scheme described above implemented with a second-generation cell model is around 0.02 ms (TenTusscher et al., 2004; Xu and Guevara, 1998). For simulations with simplified or reduced cell models, the time step can be extended to between 0.05 and 0.1 ms (Cherry and Fenton, 2004; Clayton and Holden, 2004).

An appropriate space step for the finite difference method results in smoothly curved activation wavefronts that are not distorted by the underlying grid. Typical space step values for whole-ventricle simulations are around 0.25 mm (Cherry and Fenton, 2004; Xie et al., 2004), which is close to the length of individual myocytes.

The effective diffusion coefficient is proportional to the bulk conductance of cardiac tissue (Eq. (9)) and determines the conduction velocity, which is proportional to the square root of bulk conductance (Hodgkin, 1954; Walton and Fozzard, 1983). The bulk conductance of cardiac tissue is however difficult to measure precisely, and a range of values have been used for both diffusion coefficient in monodomain simulations and conductivity tensors in bidomain simulations. Measurements of longitudinal and transverse intracellular conductivity range from 0.174 to 0.344 and 0.0193 to 0.05976 $S\,m^{-1}$, respectively (Malmivuo and Plonsey, 1995). If these measurements are taken as an approximation of bulk intracellular conductivity, then they correspond to a longitudinal diffusion coefficient $D_{||}$ of between 0.0007 and 0.0003 $cm^2\,ms^{-1}$, and a transverse diffusion coefficient $D_{\perp}$ of between 0.0001 and 0.00004 $cm^2\,ms^{-1}$ for C_m of 1 $\mu F\,cm^{-2}$ and S_v of 5000 cm^{-1} (Xu and Guevara, 1998). In practice, larger values of $D_{||}$ and $D_{\perp}$ are typically chosen, to match measured values of plane wave propagation speed along and across fibres. In ventricular tissue, measurements of longitudinal conduction velocity are typically between 0.4 and 0.6 ms^{-1} along fibres, and measurements of transverse conduction velocity are around half this value (Kleber and Rudy, 2004). A 1:2 ratio of conduction velocity implies a 1:4 ratio of diffusion coefficient, and typical choices of longitudinal and transverse diffusion coefficients are 0.001 and 0.0005 $cm^2\,ms^{-1}$ (Clayton and Holden, 2004), and 0.001 and 0.00025 $cm^2\,ms^{-1}$ (Xie et al., 2004).

An important technique for speeding up computations is operator splitting, where computation of the diffusion operator in (8) and integration of the cell model ODEs are separated (Qu and Garfinkel, 1999; Quan

et al., 1998). The time step for solving the cell model ODEs can then be made adaptive, so that a shorter time step is chosen for the action potential upstroke based on local values of dV_m/dt. This can result in significantly faster computations. The simulations shown in Fig. 3(a), where the first-generation LR1 model is embedded in a monodomain tissue model, were solved using explicit finite differences with $D = 0.1\,\mathrm{mm^2\,ms^{-1}}$, and a space step of 0.25 mm. With a fixed time step of 0.025 ms, the simulation of 3500 ms of activity on a single CPU (Pentium 4, 2.4 GHz) took 22 min 30 s. In contrast, with operator splitting and a variable time step of between 0.025 and 0.25 ms, the same simulation was complete in 3 min 18 s.

For an explicit finite difference solution to the monodomain model with isotropic diffusion, a standard stability analysis (Press et al., 1992) leads to the criterion that

$$\frac{D\Delta t}{\Delta x^2} < \frac{1}{2d}, \tag{24}$$

where Δt and Δx are the time step and space step, D the diffusion coefficient, and d the dimension of the simulation, $d = 3$ for whole-ventricle models. Instability close to this limit will often be manifest as large changes in plane wave conduction velocity with small changes in time or space step. Even if this stability criterion is fulfilled, it is still possible to choose an inappropriately large space step that gives irregular wavefront curvature (illustrated in Fig. 5(a)). This approach may result in instability of re-entrant waves that is a numerical artifact rather than a genuine property of a particular model (Fenton et al., 2002).

5.5. Boundary conditions

Many researchers have used Neumann no-flux boundary conditions for the monodomain model (Clayton and Holden, 2004; Panfilov and Keener, 1995b; Xie et al., 2004). These are $\mathbf{n} \cdot D\nabla V_m = 0$, where $\mathbf{n}$ is a vector normal to the surface. The physical interpretation of this boundary condition is that no current flows into or out of the external environment, and this approach is justified if the fibres are parallel to the heart surface, or if the fibre ends are sealed after excision of a slab. For anatomically detailed whole-ventricle models, implementation of these boundary conditions requires a computationally efficient method for estimating $\mathbf{n}$.

One approach described in Panfilov (1998) and TenTusscher and Panfilov (2007) is based on weight adjustment for boundary points. For example, for a one-dimensional cable, the Laplacian operator for each point (x,y,z) inside the cable is given by (25). This equation can be viewed as the difference of currents from the left and the right neighbouring points:

$$\left.\frac{\partial^2 V_m}{\partial x^2}\right|_{x=x_i} = \frac{1}{\Delta x}\left(\frac{V_m(x_i+1) - V_m(x_i)}{\Delta x} - \frac{V_m(x_i) - V_m(x_i-1)}{\Delta x}\right). \tag{25}$$

As a result, the weights of the point $V_m(x_i)$ and its right and left neighbours are given by $(1/\Delta x^2, -2/\Delta x^2, 1/\Delta x^2)$, where Δx is the space step. For the point at the right boundary with no-flux boundary conditions (Fig. 6(a)), there will be no current from the right end of the fibre, and the weights of these points will be $(1/\Delta x^2, -1/\Delta x^2, 0)$. In Panfilov (1998) and TenTusscher and Panfilov (2007), this method was extended to a three-dimensional anisotropic case which accounts for the boundary condition $\mathbf{n} \cdot D\Delta V_m = 0$. This method is very effective computationally, as evaluation of the Laplacian here is just an explicit matrix multiplication.

A further extension of this method of weight adjustment is the immersed interface method. Let us illustrate it on a 1D case, with the boundary located at point a (Fig. 6(b)). We can approximate a Laplacian at the boundary point a using the two closest interior points $V_i = V_m(x_i)$ and $V_{i-1} = V_m(x_i - 1)$ with weights P and Q:

$$\frac{\partial^2 V_m}{\partial x^2} = PV_{i-1} + QV_i. \tag{26}$$

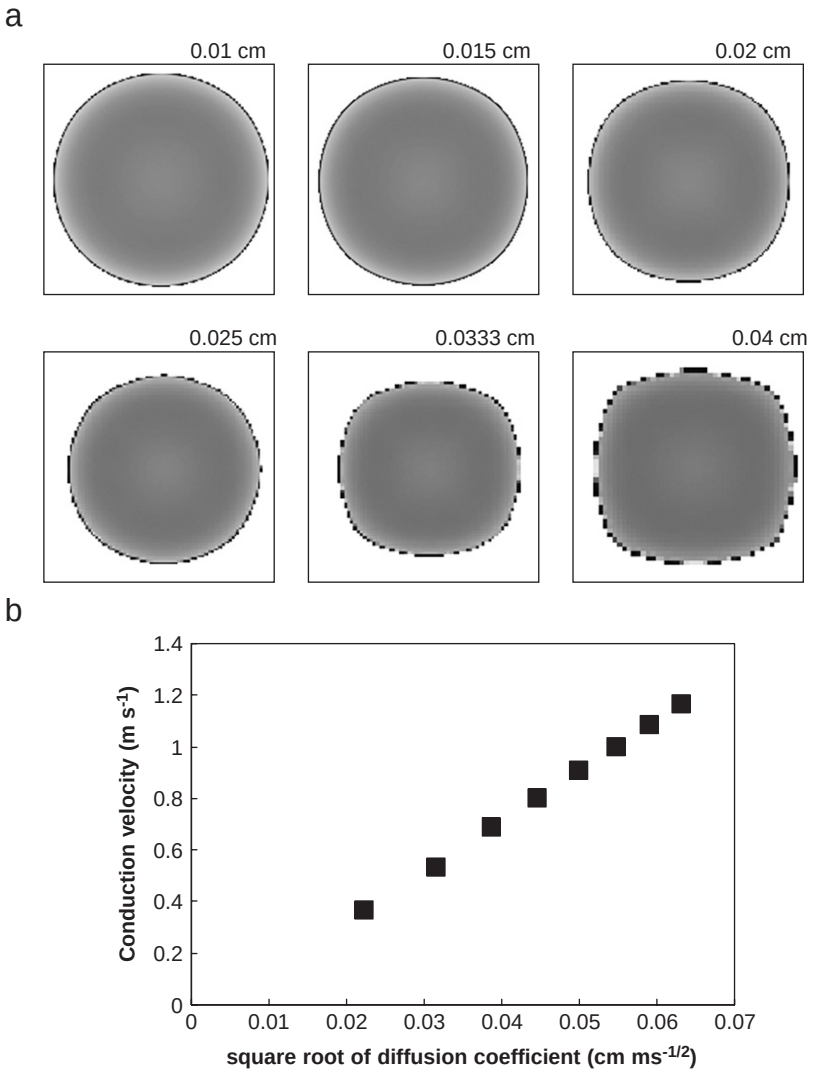

Fig. 5. (a) Spread of an action potential in a 50×50 mm 2D tissue sheet simulated using the monodomain tissue model with the LR1 cell model, solved with explicit finite differences for a diffusion coefficient of $0.001\,cm^2\,ms^{-1}$, an adaptive time step of between 0.005 and 0.25 ms, and different space steps as shown. Grey regions show spreading region of depolarised tissue resulting from a point stimulus at the centre of the sheet. (b) Dependence of conduction velocity of curved wavefronts in this model on the square root of diffusion coefficient, for a fixed space step of 0.025 cm and an adaptive time step of between 0.00625 and 0.25 ms.

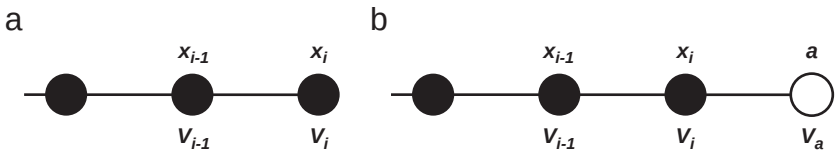

Fig. 6. No-flux boundary conditions for a one-dimensional fibre. (a) End of fibre, point x_i is at the boundary. (b) Boundary point a used to determine weighting, for estimating no-flux boundary conditions, see text for details.

If we then replace V_{i-1} and V_i with their Taylor expansions at point V_a, we get

$$\left.\frac{\partial^2 V}{\partial x^2}\right|_{x=a} = P\left[V_a + (x_i - a)\left.\frac{\partial V}{\partial x}\right|_{x=a} + \frac{1}{2}(x_i - a)^2\left.\frac{\partial^2 V}{\partial x^2}\right|_{x=a}\right] + Q\left[V_a + (x_{i-1} - a)\left.\frac{\partial V}{\partial x}\right|_{x=a} + \frac{1}{2}(x_{i-1} - a)^2\left.\frac{\partial^2 V}{\partial x^2}\right|_{x=a}\right]. \tag{27}$$

From here, if we impose no-flux boundary conditions $\partial V/\partial x|_{x=a} = 0$ we obtain the following system, which determines the weights P and Q:

$$\begin{cases} P + Q = 0, \\ P\,\frac{1}{2}(x_i - a)^2 + Q\,\frac{1}{2}(x_{i-1} - a)^2 = 1. \end{cases} \tag{28}$$

Thus

$$P^{-1} = (x_i - a)^2 - (x_{i-1} - a)^2, \quad Q = -P. \tag{29}$$

This method has been extended to a general 3D anisotropic case in Dumnet and Keener (2003).

An elegant way to avoid complex boundary conditions was used in Fenton et al. (2005), where a phase field algorithm was employed. In this approach, Eq. (8) is modified to

$$\phi\,\frac{\partial V_m}{\partial t} = \nabla(\mathbf{D}\phi\nabla V_m) - \phi\,\frac{I_{ion}}{C_m}, \tag{30}$$

where ϕ is a phase variable, which has a value of 1 for points inside the ventricles, and decays to $\phi = 0$ outside the ventricles. If the decay length is small enough, the solutions of this equation, which does not have complex boundary conditions, will be close to the solutions of Eq. (8) for a no-flux boundary condition. In Fenton et al. (2005), application of this method was demonstrated for models of anatomically detailed rabbit and canine ventricle geometry.

For the bidomain model the boundary conditions for endocardial and epicardial surfaces may vary. In the torso there is electrical continuity between the extracellular space of the heart and the surrounding tissue, but the intracellular region of cardiac tissue is electrically isolated. Appropriate boundary conditions at the heart torso interface are therefore continuity of both extracellular potential and the normal component of extracellular current, and zero normal component of intracellular current (Keener and Bogar, 1998). An advantage of the bidomain model is that it allows implementation of the so-called bath boundary condition, which is considered the most accurate one for the endocardial surface of the heart, which has direct contact with blood.

5.6. *Parallel computation using shared and distributed memory*

High-performance computational resources are becoming more widely available, and are needed for the type of whole-ventricle simulation described in this paper. For the finite difference scheme with operator splitting described above, simulation code will be structured as a time loop, with additional nested loops to update the diffusion term and the I_{ion} term at each time step. Implementing this process on a parallel computer with shared memory is a relatively straightforward process; the loops to update the diffusion term and the I_{ion} term can be divided between the processors available, and each thread has access to the state variables stored in the shared memory. With careful coding and optimisation, this approach can yield reasonable scaling up to around 16 processors. Fig. 7 shows an example of scaling. In this example, a small section of code for producing output to a file and estimating an electrocardiogram was left as serial, and the cumulative effect of this serial code can be seen as a loss of scaling with increasing numbers of processors. This phenomenon, Amdahl's law, states that when a parallel code contains a small fraction of serial code, s, then the maximum possible speedup is $1/s$ (Gustafson, 1988).

There is an increasing trend towards the use of high-performance machines with distributed memory, where each thread maintains its own copy of part of state variable space. In this approach, the division of the computational task becomes important, because the communication overhead required to update each copy of

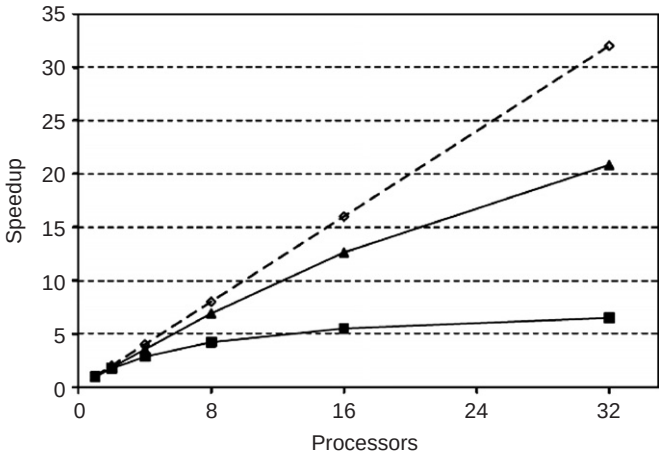

Fig. 7. Scaling of code for an explicit finite difference solution of the monodomain equation on the HPCx computational resource. Dashed line with diamonds shows ideal linear scaling, solid line with squares shows scaling before code optimisation and solid line with triangles shows scaling after code optimisation.

the state variable space must be minimised. Several publications have outlined schemes for achieving this (Pitt-Francis et al., 2006; Porras et al., 2000; Winslow et al., 2001).

5.7. Validation

Validation of any computational model is a critical aspect of its development. There are two distinct aspects to this process; first there is validation of the underlying model components at the cell, tissue and organ levels, and second there is checking of the simulation code for correctness.

Models at the cell level are generally validated during development by comparison with experimental measurements of action potential shape, and rate dependence of APD. In second-generation cardiac models, a simulated voltage-clamp experiment can be used to verify the correct behaviour of ion channel currents and gating variables against experimental data. Second-generation models can also be validated by comparison of simulated intracellular Ca^{2+} transients with experimental data, and by observing changes in the diastolic intracellular Ca^{2+} concentration at different pacing cycle lengths.

Once a code module has been developed for a particular cell model, it is important to verify the code against published data, for example action potential shape, so that any errors in the code can be identified and corrected. As noted above, the ongoing development of languages such as CellML will ease this process.

Models at the tissue level can be validated in abstract geometries against experimental data, for example the conduction velocity along and across fibres can be compared in 2D sheets and 3D slabs with and without anisotropy. One of the widely used experimental techniques for observing action potential propagation in cardiac tissue is the use of voltage-sensitive fluorescent dyes, and new techniques have been developed to synthesise these signals from tissue models (Bishop et al., 2006; Hyatt et al., 2003). Although these approaches have been developed so that three-dimensional information can be inferred from optical surface recordings, they also provide a potentially valuable tool for validating tissue models and verifying tissue code.

At the whole-ventricle level, simulated activation and recovery sequences during normal and paced beats can be compared against published data for activation and recovery. These include data for the human (Durrer et al., 1970) and canine (Scher and Spach, 1979; Taccardi et al., 2005) ventricle.

6. Conclusions and future directions

The components needed to construct whole-ventricle models of electrophysiology are now available, and this type of approach is already yielding valuable insight into the mechanisms of 3D wave propagation,

arrhythmogenesis and defibrillation in the whole ventricle. However, all of these models have limitations, and a careful choice of cell and tissue model, as well as an appropriate choice of anatomical model is important.

There are several general limitations to the approach described in this paper. Perhaps the most important of these is that the mechanical activity of the ventricles is not included in purely electrical models. During fibrillation, the mechanical activity is much reduced, and so this limitation is less important. During a normal beat, however, the electrically initiated contraction not only changes the cell and tissue geometry (Smith et al., 2003), but also feeds back to electrical activity through the action of mechano-sensitive ion channels (Kohl et al., 1999). These effects are most notable during electrical repolarisation. Other limitations that have already been discussed include those of the models at the cell and tissue levels.

Nevertheless, there are many research questions that will be answered in part by the use of whole-ventricle models of electrophysiology. The mechanism of defibrillation has already been probed in detail using this approach (Trayanova, 2006). Among the many remaining questions are the role of ventricular anatomy in determining the complexity of fibrillation, and the influence of structural (fibroblasts, vessels, sheets), functional (regional expression of ion channels, mechanics) and pathophysiological heterogeneity on normal and abnormal activation patterns. With an increased emphasis on the development of carefully validated, correct and efficient codes for whole-ventricle simulations, we look forward to exciting developments in this area.

Acknowledgements

RHC gratefully acknowledges funding from the British Heart Foundation (BS 98001, PG/03/102/1582), and is also grateful to both the White Rose Grid (www.wrgrid.org.uk) and the Integrative Biology eScience project (EPSRC Grant no. GR/572023/01) for providing computational resources. Flavio Fenton and Elizabeth Cherry provided parameter sets for the 4-variable model shown in Fig. 3(e), and Michael Holden at Edinburgh Parallel Computer Centre produced the data shown in Fig. 7. The paper was written during the stay of AVP at IHES. He is thankful to the IHES for their hospitality and support. This work was also supported by the Netherlands Organisation for Scientific Research (NWO) through grant number 635100004 of the Research Council for Physical Sciences (AVP).

References

Aliev, R.R., Panfilov, A.V., 1996. A simple two-variable model of cardiac excitation. Chaos Solitons Fractals 7, 293–301.

Aslanidi, O.V., Bailey, A., Clayton, R.H., Holden, A.V., 2002. Enhanced self-termination of re-entrant arrhythmias as a pharmacological strategy for antiarrhythymic action. Chaos 12, 843–851.

Austin, T., Hooks, D., Hunter, P., Nickerson, D., Pullan, A., Sands, G., Smaill, B., Trew, M., 2006. Modeling cardiac electrical activity at the cell and tissue levels. Ann NY Acad Sci 1080, 334–347.

Banville, I., Gray, R.A., 2002. Effect of action potential duration and conduction velocity restitution on alternans and the stability of arrhythmias. J Cardiovasc Electrophysiol 13, 1141–1149.

Beeler, G.W., Reuter, H., 1977. Reconstruction of the action potential of ventricular myocardial fibres. J Physiol 268, 177–210.

Berenfeld, O., Pertsov, A.M., 1999. Dynamics of intramural scroll waves in three-dimensional continuous myocardium with rotational anisotropy. J Theor Biol 199, 383–394.

Bers, D.M., 2002. Cardiac excitation–contraction coupling. Nature 415, 198–205.

Bers, D.M., Guo, T., 2005. Calcium signalling in cardiac ventricular myocytes. Ann NY Acad Sci 1047, 86–98.

Bishop, M.J., Rodriguez, B., Eason, J.C., Whiteley, J.P., Trayanova, N., Gavaghan, D.J., 2006. Systhesis of voltage-sensitive optical signals: application to panoramic optical mapping. Biophys J 90, 2938–2945.

Boyett, M.R., Jewell, B.R., 1980. Analysis of the effects of changes in rate and rhythm on electrical activity in the heart. Progr Biophys Molec Biol 36, 1–52.

Boyett, M.R., Harrison, S.M., Janvier, N.C., McMorn, S.O., Owen, J.M., Shui, Z., 1996. A list of vertebrate cardiac ionic currents nomenclature, properties, function and cloned equivalents. Cardiovasc Res 32, 455–481.

Bub, G., Shrier, A., Glass, L., 2002. Spiral wave generation in heterogenous excitable media. Phys Rev Lett 88, 058101-1–058101-4.

Buist, M., Sands, G., Hunter, P., Pullan, A., 2003. A deformable finite element derived finite difference method for cardiac activation problems. Ann Biomed Eng V 31, 577–588.

Burton, R.A.B., Plank, G., Schneider, J.E., Grau, V., Ahammer, H., Keeling, S.J., Lee, J., Smith, N.P., Gavaghan, D., Trayanova, N., Kohl, P., 2006. 3-Dimensional models of individual cardiac histo-anatomy: tools and challenges. Ann NY Acad Sci 1380, 301–319.

Camelleti, P., Borg, T.K., Kohl, P., 2005. Structural and functional characterisation of cardiac fibroblasts. Cardiovasc Res 65, 40–51.

Carmeliet, E., 1999. Cardiac ion currents and acute ischaemia: from channels to arhythmias. Physiol Rev 79, 917–1017.
Chavez, F., Kapral, R., Rousseau, G., Glass, L., 2001. Scroll waves in spherical shell geometries. Chaos 11, 757–765.
Chen, X., Fenton, F.H., Gray, R.A., 2005. Head–tail interactions in numerical simulations of reentry in a ring of cardiac tissue. Heart Rhythm 2, 851–859.
Cherry, E., Fenton, F., 2004. Suppression of alternans and conduction blocks despite steep APD restitution: electrotonic, memory, and conduction velocity restitution effects. Am J Physiol (Heart Circ Physiol) 286, 2332–2341.
Cherry, E.M., Fenton, F.H., 2007. A tale of two dogs: analyzing two models of canine ventricular electrophysiology. Am J Physiol (Heart Circ Physiol) 292, H43–H55.
Clancy, C.E., Rudy, Y., 1999. Linking a genetic defect to its cellular phenotype in a cardiac arrhythmia. Nature 400, 566–569.
Clancy, C.E., Rudy, Y., 2001. Cellular consequences of HERG mutations in the long QT syndrome: precursors to sudden cardiac death. Cardiovasc Res 50, 301–313.
Clayton, R.H., Holden, A.V., 2002. A method to quantify the dynamics and complexity of re-entry in computational models of ventricular fibrillation. Phys Med Biol 47, 225–238.
Clayton, R.H., Holden, A.V., 2003. Effect of regional differences in cardiac cellular electrophysiology in the stability of ventricular arrhythmias: a computational study. Phys Med Biol 48, 95–111.
Clayton, R.H., Holden, A.V., 2004. Filament behaviour in a computational model of ventricular fibrillation in the canine heart. IEEE Trans Biomed Eng 51, 28–34.
Clayton, R.H., Taggart, P., 2005. Regional differences in APD restitution can initiate wavebreak and re-entry in cardiac tissue: a computational study. Biomed Eng OnLine 4, 54.
Clayton, R.H., Zhuchkova, E.A., Panfilov, A., 2006. Phase singularities and filaments: simplifying complexity in computational models of ventricular fibrillation. Progr Biophys Molec Biol 90, 378–398.
Colli Franzone, P., Pavarino, L.F., Taccardi, B., 2006. Effects of transmural electrical heterogeneities and electrotonic interactions on the dispersion of cardiac repolarization and action potential duration: a simulation study. Math Biosci 204, 132–165.
Conrath, C.E., Wilders, R., Coronel, R., De Bakker, J.M.T., Taggart, P., De Groot, J.R., Opthof, T., 2004. Intercellular coupling through gap junctions masks M cells in the human heart. Cardiovasc Res 62.
DiFrancesco, D., Noble, D., 1985. A model of cardiac electrical activity incorporating ionic pumps and concentration changes. Philos Trans R Soc Lond B 307, 353–398.
dos Santos, R.W., Plank, G., Bauer, S., Vigmond, E.J., 2004. Parallel multigrid preconditioner for the cardiac bidomain model. Biomed Eng IEEE Trans 51, 1960–1968.
Dumnet, M., Keener, J.P., 2003. A numerical method for solving anisotropic elliptic boundary problems in 3D. SIAM J Sci Comput 25, 348–367.
Durrer, D., Dam, R.T.v., Freud, G.E., Janse, M.J., Meijler, F.L., Arzbaecher, R.C., 1970. Total excitation of the isolated human heart. Circulation 41, 899–912.
Eisner, D.A., Choi, H.S., Diaz, M.E., O'Neill, S.C., Trafford, A.W., 2000. Integrative analysis of calcium cycling in cardiac muscle. Circ Res 87, 1087–1094.
Faber, G.M., Rudy, Y., 2000. Action potential and contractility changes in Na+ (i) overloaded cardiac myocytes: a simulation study. Biophys J 78, 2392–2404.
Fenton, F., Karma, A., 1998. Vortex dynamics in three-dimensional continuous myocardium with fibre rotation: filament instability and fibrillation. Chaos 8, 20–47.
Fenton, F., Cherry, E., Karma, A., Rappel, W.-J., 2005. Modeling wave propagation in realistic heart geometries using the phase-field method. Chaos 15, 013502.
Fenton, F.H., Cherry, E.M., Hastings, H.M., Evans, S.J., 2002. Multiple mechanisms of spiral wave breakup in a model of cardiac electrical activity. Chaos 12, 852–892.
Ferrero, J.M.J., Trenor, B., Rodriguez, B., Saiz, J., 2003. Electrical activity and re-entry during acute regional ischaemia: insights from simulations. Int J Bifurc Chaos 13, 3703–3716.
Fitzhugh, R., 1961. Impulses and physiological states in theoretical models of nerve membrane. Biophys J 1, 445–466.
Fox, J.J., McHarg, J.L., Gilmour, R.F., 2002. Ionic mechanism of electrical alternans. Am J Physiol (Heart Circ Physiol) 282, H516–H530.
Franz, M.R., 2003. The electrical restitution curve revisited: steep or flat slope-which is better? J Cardiovasc Electrophysiol 14, S140–S147.
Garfinkel, A., Kim, Y.H., Voroshilovsky, O., Qu, Z.L., Kil, J.R., Lee, M.H., Karagueuzian, H.S., Weiss, J.N., Chen, P.S., 2000. Preventing ventricular fibrillation by flattening cardiac restitution. Proc Natl Acad Sci USA 97, 6061–6066.
Geerts, L., Bovendeerd, P., Nicolay, K., Arts, T., 2002. Characterization of the normal cardiac myofiber field in goat measured with MR-diffusion tensor imaging. Am J Physiol (Heart Circ Physiol) 283, H139–H145.
Gima, K., Rudy, Y., 2002. Ionic current basis of electrocardiographic waveforms. A model study. Circ Res 90, 889–896.
Gray, R.A., Jalife, J., 1998. Ventricular fibrillation and atrial fibrillation are two different beasts. Chaos 8, 65–78.
Gulrajani, R.M., 1998. Bioelectricity and Biomagnetism. Wiley, New York.
Gustafson, J.L., 1988. Re-evaluating Amdahl's law. ACM Commun 31, 532–533.
Harrild, D.M., Penland, R.C., Henriquez, C.S., 2000. A flexible method for simulating cardiac conduction in three-dimensional complex geometries. J Electrocardiol 33, 241–251.
Helm, P., Faisal, M., Miller, M.I., Winslow, R.L., 2005. Measuring and mapping cardiac fiber and laminar architecture using diffusion tensor imaging. Ann NY Acad Sci 1047, 296.

Henriquez, C.S., Papazogou, A.A., 1996. Using computer models to understand the roles of tissue structure and membrane dynamics in arrhythmogenesis. Proc IEEE 84, 334–354.

Henriquez, C.S., Tranquillo, J.V., Weinstein, D., Hsu, E.W., Johnson, C.R., 2004. Three dimensional propagation in mathematic models: integrative model of the mouse heart. In: Zipes, D.P., Jalife, J. (Eds.), Cardiac Electrophysiology from Cell to Bedside. Saunders, Philadelphia, pp. 273–281.

Hodgkin, A.L., 1954. A note on conduction velocity. J Physiol 125, 221–224.

Hodgkin, A.L., Huxley, A.F., 1952. A quantitative description of membrane current and its application to conduction and excitation in nerve. J Physiol (London) 117, 500–544.

Hooks, D.A., Tomlinson, K.A., Marsden, S.G., LeGrice, I.J., Smaill, B.H., Pullan, A., 2002. Cardiac microstructure: implications for electrical propagation and defibrillation in the heart. Circ Res 91, 331–338.

Hren, R., Nenonen, J., Horacek, B.M., 1998. Simulated epicardial potential maps during paced activation reflect myocardial fibrous structure. Ann Biomed Eng 26.

Hsu, E.W., Muzikant, A.L., Matulevicius, S.A., Penland, R.C., Henriquez, C.S., 1998. Magnetic resonance myocardial fiber-orientation mapping with direct histological correlation. Am J Physiol (Heart Circ Physiol) 274, 1627–1634.

Hund, T.J., Rudy, Y., 2004. Rate dependence and regulation of action potential and calcium transient in a canine cardiac ventricular cell model. Circulation 110, 4008–4074.

Hund, T.J., Kucera, J.P., Otani, N.F., Rudy, Y., 2001. Ionic charge conservation and long-term steady state in the Luo–Rudy dynamic model. Biophys J 81, 3324–3331.

Hyatt, C.J., Mironov, S.F., Wellner, M., Berenfeld, O., Popp, A.K., Weitz, D.A., Jalife, J., Pertsov, A.M., 2003. Synthesis of voltage-sensitive fluorescence signals from three-dimensional myocardial activation patterns. Biophys J 85, 2673–2683.

Keener, J.P., Bogar, K., 1998. A numerical method for the solution of the bidomain equations in cardiac tissue. Chaos 8, 234–241.

Keener, J.P., Sneyd, J., 1998. Mathematical Physiology. Springer, New York.

Kleber, A.G., Rudy, Y., 2004. Basic mechanisms of cardiac impulse propagation and associated arrhythmias. Physiol Rev 84, 431–488.

Kohl, P., Hunter, P.J., Noble, D., 1999. Stretch-induced changes in heart rate and rhythm: clinical observations, experiments and mathematical models. Progr Biophys Molec Biol 71, 91–138.

Le Bihan, D., Mangin, J.-F., Poupon, C., Clark, C.A., Pappata, S., Molko, N., Chabriat, H., 2001. Diffusion tensor imaging: concepts and applications. J Magn Reson Imag 13, 534–546.

LeGrice, I.J., Smaill, B.H., Chai, L.Z., Edgar, S.G., Gavin, J.B., Hunter, P.J., 1995. Laminar structure of the heart: ventricular myocyte arrangement and connective tissue architecture in the dog. Am J Physiol (Heart Circ Physiol) 269, 571–582.

LeGrice, I.J., Hunter, P.J., Young, A.A., Smaill, B.H., 2001. The architecture of the heart: a data based model. Philos Trans R Soc Lond A 359, 1217–1232.

Lloyd, C.M., Halstead, M.D., Nielsen, P.F., 2004. CellML: its future, present, and past. Progr Biophys Molec Biol 85, 433–450.

Luo, C.-H., Rudy, Y., 1991. A model of the ventricular cardiac action potential. Depolarization, repolarization and their interaction. Circulation 68, 1501–1526.

Luo, C.H., Rudy, Y., 1994. A dynamic-model of the cardiac ventricular action-potential. 1. Simulations of ionic currents and concentration changes. Circ Res 74, 1071–1096.

Malmivuo, J., Plonsey, R., 1995. Bioelectromagnetism. Principles and Applications of Bioelectric and Biomagnetic Fields. Oxford University Press, New York.

Matsuoka, S., Sarai, N., Kuratomi, S., Ono, K., Noma, A., 2003. Role of individual ionic current systems in ventricular cells hypothesised by a model study. Jpn J Physiol 53, 105–123.

McAllister, R.E., Noble, D., Tsien, R.W., 1975. Reconstruction of the electrical activity of cardiac Purkinje fibres. J Physiol 251, 1–59.

Miller, W., Geselowitz, D., 1978. Simulation studies of the electrocardiogram. I. The normal heart. Circ Res 43, 301–315.

Moe, G.K., Rheinboldt, W.C., Abildskov, J.A., 1964. A computer model of atrial fibrillation. Am Heart J 67, 200–220.

Nickerson, D.P., Hunter, P.J., 2006. The noble cardiac ventricular electrophysiology models in CellML. Progr Biophys Molec Biol 90, 346–359.

Nielsen, P.M., Le Grice, I.J., Smaill, B.H., Hunter, P.J., 1991. Mathematical model of geometry and fibrous structure of the heart. Am J Physiol (Heart Circ Physiol) 260, 1365–1378.

Noble, D., 1962. A modification of the Hodgkin–Huxley equations applicable to Purkinje fibre action and pace-maker potentials. J Physiol 160, 317–352.

Noble, D., Rudy, Y., 2001. Models of cardiac ventricular action potentials: iterative interaction between experiment and simulation. Philos Trans R Soc Lond Ser A Math Phys Eng Sci 359, 1127–1142.

Noble, D., Varghese, A., Kohl, P., Noble, P., 1998. Improved guinea pig ventricular cell model incorporating a dyadic space, IKr and IKs, and length and tension dependent processes. Can J Cardiol 14, 123–134.

Okajima, M., Fujino, T., Kobayashi, T., Yamada, K., 1968. Computer simulation of the propagation process in excitation of the ventricles. Circ Res 23, 203–211.

Pandit, S.V., Clark, R.B., Giles, W.R., Demir, S.S., 2001. A mathematical model of action potential heterogeneity in adult rat left ventricular myocytes. Biophys J 81, 3029–3051.

Panfilov, A.V., 1997. Modeling propagating activity in an anatomical model of the ventricle. In: Holden, A.V., Panfilov, A.V. (Eds.), Computational Biology of the Heart. Wiley, Chichester, pp. 259–276.

Panfilov, A.V., 1998. Spiral breakup as a model of ventricular fibrillation. Chaos 8, 57–64.

Panfilov, A.V., 1999. Three-dimensional organization of electrical turbulence in the heart. Phys Rev E 59, R6251–R6254.

Panfilov, A.V., Keener, J.P., 1993. Generation of reentry in anisotropic myocardium. J Cardiovasc Electrophysiol 4, 412–421.

Panfilov, A.V., Keener, J.P., 1995a. Re-entry in an anatomical model of the heart. Chaos Solitons Fractals 5, 681–689.
Panfilov, A.V., Keener, J.P., 1995b. Re-entry in three-dimensional Fitzhugh–Nagumo medium with rotational anisotropy. Physica D 84, 545–552.
Pitt-Francis, J., Garny, A., Gavaghan, D., 2006. Enabling computer models of the heart for high performance computers and the grid. Philos Trans R Soc A 364, 1501–1516.
Porras, D., Rogers, J.M., Smith, W.M., Pollard, A.E., 2000. Distributed computing for membrane-based modeling of action potential propagation. IEEE Trans Biomed Eng 47, 1051–1057.
Press, W.H., Flannery, B.P., Teukolsky, S.A., Vetterling, W.T., 1992. Numerical Recipes in C. The Art of Scientific Computing. Cambridge University Press, Cambridge.
Priebe, L., Beuckelmann, D.J., 1998. Simulation study of cellular electrical properties in heart failure. Circ Res 82, 1206–1223.
Puglisi, J.L., Bers, D.M., 2001. LabHEART: an interactive computer model of rabbit ventricular myocyte ion channels and Ca transport. Am J Physiol (Heart Circ Physiol) 281, C2049–C2060.
Puglisi, J.L., Wang, F., Bers, D.M., 2004. Modelling the isolated cardiac myocyte. Progr Biophys Molec Biol 85, 163–178.
Qu, Z.L., Garfinkel, A., 1999. An advanced algorithm for solving partial differential equation in cardiac conduction. IEEE Trans Biomed Eng 46, 1166–1168.
Qu, Z.L., Weiss, J.N., Garfinkel, A., 1999. Cardiac electrical restitution properties and stability of reentrant spiral waves: a simulation study. Am J Physiol (Heart Circ Physiol) 276, H269–H283.
Qu, Z.L., Kil, K., Xie, F.G., Garfinkel, A., Weiss, J.N., 2000. Scroll wave dynamics in a three-dimensional cardiac tissue model: roles of restitution, thickness, and fiber rotation. Biophys J 78, 2761–2775.
Quan, W., Evans, S.J., Hastings, H.M., 1998. Efficient integration of a realistic two-dimensional cardiac tissue model by domain decomposition. IEEE Trans Biomed Eng 45, 372–385.
Roden, D.M., Balser, J.R., George, A.L.J., Anderson, M.E., 2002. Cardiac ion channels. Annu Rev Physiol 64, 431–475.
Rodriguez, B., Eason, J.C., Trayanova, N., 2006. Differences between left and right ventricular anatomy determine the types of reentrant circuits induced by an external electric shock. A rabbit heart simulation study. Progr Biophys Molec Biol 90, 399–413.
Rogers, J.M., 2002. Wave front fragmentation due to ventricular geometry in a model of the rabbit heart. Chaos 12, 779–787.
Rogers, J.M., McCulloch, A.D., 1994. A collocation-Galerkin finite element model of cardiac action potential propagation. IEEE Trans Biomed Eng 41, 743–757.
Rohlf, K., Glass, L., Kapral, R., 2006. Spiral wave dynamics in excitable media with spherical geometries. Chaos (Woodbury NY) 16, 037115.
Roth, B.J., 2004. Art Winfree and the bidomain model of cardiac tissue. J Theor Biol 230, 445–449.
Rudy, Y., 2006. Computational biology in the study of cardiac ion channels and cell electrophysiology. Q Rev Biophys 39, 57–116.
Rush, S., Larsen, H., 1978. A practical algorithm for solving dynamic membrane equations. IEEE Trans Biomed Eng 25, 389–392.
Sambelashvilli, A., Efimov, I.R., 2004. Dynamics of virtual electrode-induced scroll-wave reentry in a 3D bidomain model. Am J Physiol (Heart Circ Physiol) 287, H1570–H1581.
Sampson, K.J., Henriquez, C.S., 2005. Electrotonic influences on action potential duration dispersion in small hearts: a simulation study. Am J Physiol (Heart Circ Physiol) 289, H350–H360.
Scher, A.M., Spach, M.S., 1979. Cardiac depolarisation and repolarisation and the electrocardiogram. In: Handbook of Physiology—The Cardiovascular System, Vol. 1. American Physiological Society, Baltimore, pp. 357–392.
Scollan, D.F., Holmes, A., Zhang, J., Winslow, R.L., 2000. Reconstruction of cardiac ventricular geometry and fibre orientation using magnetic resonance imaging. Ann Biomed Eng 28, 934–944.
Sermesant, M., Delingette, H., Ayache, N.Y., 2006. An electromechanical model of the heart for image analysis and simulation. IEEE Trans Med Imag 25, 612–625.
Shaw, R.M., Rudy, Y., 1997. Electrophysiologic effects of acute myocardial ischemia—a mechanistic investigation of action potential conduction and conduction failure. Circ Res 80, 124–138.
Smith, N.P., Buist, M.L., Pullan, A.J., 2003. Altered T wave dynamics in a contracting cardiac model. J Cardiovasc Electrophysiol 14, S203–S209.
Soeller, C., Cannell, M.B., 2004. Analysing cardiac excitation–contraction coupling with mathematical models of local control. Progr Biophys Molec Biol 85, 141–162.
Stevens, C., Remme, E., LeGrice, I.J., Hunter, P.J., 2003. Ventricular mechanics in diastole: material parameter sensitivity. J Biomech 36, 737–748.
Stinstra, J.G., Hopenfeld, B., MacLeod, R.S., 2005. On the passive cardiac conductivity. Ann Biomed Eng V 33, 1743–1751.
Streeter, D.D., 1979. Gross morphology and fibrous structure of the heart. In: Handbook of Physiology—The Cardiovascular System, Vol. 1. American Physiological Society, Baltimore, pp. 61–112.
Taccardi, B., Punske, B., Sachse, F., Tricoche, X., Colli-Franzone, P., Pavarino, L., Zabawa, C., 2005. Intramural activation and repolarization sequences in canine ventricles. Experimental and simulation studies. J Electrocardiol 38, 131–137.
TenTusscher, K.H.W.J., Panfilov, A.V., 2006. Cell model for efficient simulation of wave propagation in human ventricular tissue under normal and pathological conditions. Phys Med Biol 51, 6141–6156.
TenTusscher, K.H.W.J., Panfilov. A.V., 2007. Modelling of the ventricular conduction system. Progr Biophys Molec Biol, this issue, doi:10.1016/j.pbiomolbio.2007.07.026.
TenTusscher, K.H.W.J., Noble, D., Noble, P.J., Panfilov, A.V., 2004. A model for human ventricular tissue. Am J Physiol (Heart Circ Physiol) 286, H1573–H1589.
Trayanova, N., 2006. Defibrillation of the heart: insights into mechanisms from modelling studies. Exp Physiol 91, 323–337.

Trew, M., Grice, I.L., Smaill, B., Pullan, A., 2005. A finite volume method for modeling discontinuous electrical activation in cardiac tissue. Ann Biomed Eng V 33, 590–602.

Usyk, T.P., LeGrice, I.J., McCulloch, A.D., 2002. Computational model of three-dimensional cardiac electromechanics. Comput Visual Sci 4, 249–257.

Van Cappelle, F.J.L., Durrer, D., 1980. Computer simulation or arrhythmias in a network of coupled excitable elements. Circ Res 47, 454–466.

Vetter, F.J., McCulloch, A.D., 1998. Three dimensional analysis of regional cardiac function: a model of rabbit ventricular anatomy. Progr Biophys Molec Biol 69, 157–183.

Vigmond, E., Aguel, F., Trayanova, N., 2002. Computational techniques for solving the bidomain equations in three dimensions. IEEE Trans Biomed Eng 49, 1260–1269.

Vigmond, E.J., Weber dos Santos, R., Prassl, A.J., Deo, M., Plank, G., 2007. Solvers for the cardiac bidomain equations. Progr Biophys Molec Biol, this issue, doi:10.1016/j.pbiomolbio.2007.07.012.

Viswanathan, P.C., Rudy, Y., 1999. Pause induced early afterdepolarizations in the long-QT syndrome: a simulation study. Cardiovasc Res 42, 530–542.

Viswanathan, P.C., Shaw, R.M., Rudy, Y., 1999. Effects of I-Kr and I-Ks heterogeneity on action potential duration and its rate dependence—a simulation study. Circulation 99, 2466–2474.

Walton, M.K., Fozzard, H.A., 1983. The conducted action potential: models and comparison to experiments. Biophys J 44, 9–26.

Wei, D., Okazaki, O., Harumi, K., Harasawa, H., Hosaka, H., 1995. Comparative simulation of excitation and body surface electrocardiogram with isotropic and anisotropic computer heart models. IEEE Trans Biomed Eng 42, 343–357.

Winfree, A.T., 1991. Varieties of spiral wave behaviour in excitable media. Chaos 1, 303–334.

Winslow, R.L., Rice, J., Jafri, S., Marban, E., O'Rourke, B., 1999. Mechanisms of altered excitation–contraction coupling in canine tachycardia-induced heart failure, II Model studies. Circ Res 84, 571–586.

Winslow, R.L., Scollan, D.F., Holmes, A., Yung, C.K., Zhang, J., Jafri, M.S., 2000. Electrophysiological modeling of cardiac ventricular function: from cell to organ. Annu Rev Bioeng 2, 119–155.

Winslow, R.L., Scollan, D.F., Greenstein, J.L., Yung, C.K., Baumgartner Jr., W., Bhanot, G., Gresh, D.L., Rogowitz, B.E., 2001. Mapping, modeling, and visual exploration of structure–function relationships in the heart. IBM Syst J 40, 342–359.

Xie, F., Qu, Z.L., Yang, J., Baher, A., Weiss, J.N., Garfinkel, A., 2004. A simulation study of the effects of cardiac anatomy in ventricular fibrillation. J Clin Invest 113, 686–693.

Xu, A., Guevara, M.R., 1998. Two forms of spiral-wave re-entry in an ionic model of ischaemic myocardium. Chaos 8, 157–174.

Zeng, J.L., Rudy, Y., 1995. Early afterdepolarizations in cardiac myocytes—mechanism and rate dependence. Biophys J 68, 949–964.

Zhukov, L., Barr, A.H., 2003. Heart-muscle fiber reconstruction from diffusion tensor MRI. Proceedings of the 14th IEEE Visualisation 2003 (Vis03), p. 79.